CrystEngComm

Accepted Manuscript

ROYAL SOCIETY OF CHEMISTRY

www.rsc.org/crystengcomm

Journal Name

RSCPublishing

ARTICLE

Pillared-bilayer zinc(II)–organic laminae: pore modification and selective gas adsorption

Cite this: DOI: 10.1039/x0xx00000x

Li-Wei Lee,[ab] Tzuoo-Tsair Luo,[a] Sheng-Han Lo,[a] Gene-Hsiang Lee,[d] Shie-Ming Peng,[d] Yen-Hsiang Liu,*[c] Sheng-Long Lee*[b] and Kuang-Lieh Lu*[a]

Received ooth January 2015,
Accepted ooth January 2015

DOI: 10.1039/x0xx00000x

www.rsc.org/

Three porous metal–organic frameworks, $\{[Zn_2(azpy)(aip)_2]\cdot 2DMF\}_n$ (**1**, azpy = 4,4'-azobipyridine, H_2aip = 5-aminoisophthalic acid), $\{[Zn_2(dipytz)(aip)_2]\cdot 1.15DMF\cdot 0.85MeOH\}_n$ (**2**, dipytz = di-3,6-(4-pyridyl)-1,2,4,5-tetrazine) and $\{[Zn_2(tpim)(aip)_2]\cdot 2.5DMF\cdot 2H_2O\}_n$ (**3**, tpim = 2,4,5-tri(4-pyridyl)-imidazole) were synthesized under mild conditions. All of the compounds consisted of a honeybomb-like layer, $[Zn(aip)]_n$, further pillared by N-donor ligands to form two-dimensional (2D) porous pillared-bilayer frameworks with 1D channels created inside the bilayers (4.1 × 10.1 $Å^2$ for **1**, 4.1 × 11.4 $Å^2$ for **2**, and 5.1 × 9.8 $Å^2$ for **3**, respectively). The resulting MOFs showed different pore volumes and channel shapes depending on the length and shape of the pillar ligands (35.7%, 41.7%, and 33.9% for **1**–**3**, respectively). The pore volume in **3** decreased due to the presence of the uncoordinated pyridyl group of the tpim ligand. The frameworks of **1** and **2** show the flexible properties upon solvent-exchanged processes and their CO_2 properties are different. This latter property is affected by the functional groups of the linear pillar ligand (–N=N– and tetrazine group). In particular, compound **3** possesses less flexibility through the solvent-exchanged process and preferentially absorbs CO_2 more efficiently than H_2 and N_2.

Introduction

Metal–organic frameworks (MOFs) have attracted considerable attention, not only due to their intriguing structural topologies,[1] but also because of their designable properties and potential applications in gas storage/separation,[2] catalysis,[3] sensing,[4] etc. Employing rational design strategies in constructing porous MOFs with high surface areas, predictable structures, tunable pore sizes, and functionality are among the most compelling challenges to date. In particular, pillared-bilayer porous MOFs are very rare in comparison with many published pillared-layer structures mainly due to the lack of a systematic synthetic strategy.[5] We envisaged that a tetrahedral metal centre, i.e. Zn^{2+} in combination with tridentate ligands might produce a layered structure with a vacant site in each metal centre. Followed by the coordination of a ditopic functional ligand as a pillar linker, this may result in the formation of a pillared-bilayer MOFs in reasonable yield.[6] Herein, we report on the successful preparation of three Zn(II)-based pillared-bilayer MOFs by following this synthetic method (Scheme 1). In addition, by introducing pillar ligands with different sizes, shapes and functional groups, the pore size and the flexibility of the pillared-bilayer structures can be tuned.[7] These unusual structural characteristics allow the pillared-bilayer MOFs to serve as excellent models for studies of gas adsorption properties.

Scheme 1 Design and synthesis of the pillared-bilayer frameworks **1**–**3**.

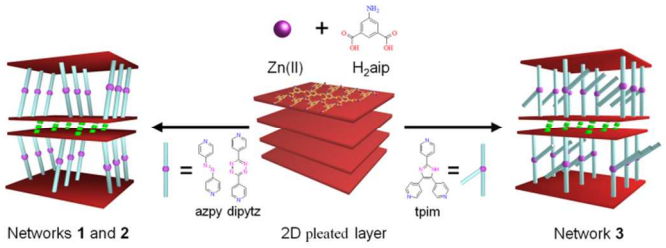

Experimental section

Materials and general methods

All reagents and solvents were purchased from commercial sources and used as received without further purification. 4,4'-azobipyridine (azpy),[8] di-3,6-(4-pyridyl)-1,2,4,5-tetrazine (dipytz)[9] and 2,4,5-tri(4-pyridyl)-imidazole (tpim)[10] were prepared according to literature methods. Infrared spectra were recorded from KBr pellets in the 4000–400 cm^{-1} range on a

Table 1 Summary of crystal data and structure refinement for **1–3**

Compound	**1**	**2**	**3**
Empirical formula	$C_{16}H_{16}N_4O_5Zn$	$C_{32.3}H_{29.45}N_{9.15}O_{10}Zn_2$	$C_{41.5}H_{44.5}N_{9.5}O_{12.5}Zn_2$
Fw	409.70	836.54	1007.11
Crystal system	Monoclinic	Monoclinic	Monoclinic
Space group	$P2_1/c$	$P2_1/c$	$P2_1/n$
a, Å	14.521(3)	16.9909(15)	16.0364(6)
b, Å	7.7378(15)	7.6688(7)	7.6528(3)
c, Å	15.997(3)	16.0077(15)	35.3947(14)
α/°	90	90	90
β/°	106.40(3)	102.322(2)	99.7638(13)
γ/°	90	90	90
V/Å^3	1724.3(6)	2037.8(3)	4280.8(3)
Z	4	2	4
λ/Å	0.71073	0.71073	0.71073
D_{calc}/g cm^{-3}	1.578	1.363	1.563
μ/mm^{-1}	1.460	1.238	1.198
F(000)	840	855	2080
GOF	1.079	1.136	1.022
$R_1{}^a$, $wR_2{}^b$ [$I > 2\sigma(I)$]	0.0424, 0.0988	0.0851, 0.2369	0.0518, 0.1497
$R_1{}^a$, $wR_2{}^b$ (all data)	0.0535, 0.1034	0.1240, 0.2651	0.0852, 0.1744

$^aR_1 = \Sigma \mid\mid F_o| - |F_c \mid\mid / \Sigma|F_o|$; $^bwR_2 = \{\Sigma[w(F_o^2 - F_c^2)^2]/\Sigma[w(F_o^2)^2]\}^{1/2}$

Table 2 Selected bond lengths (Å) and angles (°) for **1–3**

1			
Zn(1)–O(1)	1.942(2)	Zn(1)–O(3)#4	1.993(2)
Zn(1)–N(1) #5	2.058(3)	Zn(1)–N(2)	2.02(2)
O(1)–Zn(1)–O(3)#4	102.47(8)	O(1)–Zn(1)–N(1)#5	112.75(10)
O(3)#4–Zn(1)–N(2)	122.3(3)	O(1)–Zn(1)–N(2)	103.4(5)
N(2)–Zn(1)–N(1)#5	108.0(2)	O(3)#4–Zn(1)–N(1)#5	107.84(10)
2			
Zn(1)–O(1)	1.938(5)	Zn(1)–O(3)#1	1.995(6)
Zn(1)–N(2)	2.029(7)	Zn(1)–N(1)#2	2.057(7)
O(1)–Zn(1)–O(3)#1	100.5(2)	O(1)–Zn(1)–N(1)#2	114.3(3)
O(1)–Zn(1)–N(2)	101.4(3)	O(3)#1–Zn(1)–N(1)#2	106.7(3)
O(3)#1–Zn(1)–N(2)	123.9(3)	N(2)–Zn(1)–N(1)#2	109.9(3)
3			
Zn(1)–O(7)	1.943(3)	Zn(2)–O(3)	1.940(3)
Zn(1)–O(1)	1.983(3)	Zn(2)–O(6)#3	2.000(3)
Zn(1)–N(5)	2.038(4)	Zn(2)–N(2)#4	2.055(4)
Zn(1)–N(1)#1	2.052(4)	Zn(2)–N(6)#2	2.103(13)
O(7)–Zn(1)–O(1)	100.09(12)	O(3)–Zn(2)–O(6)#3	99.86(12)
O(7)–Zn(1)–N(5)	99.83(14)	O(3)–Zn(2)–N(2)#4	117.78(14)
O(1)–Zn(1)–N(5)	123.46(14)	O(6)#3–Zn(2)–N(6)#2	117.5(3)
O(7)–Zn(1)–N(1)#1	109.63(14)	O(6)#3–Zn(2)–N(2)#4	104.50(14)
O(1)–Zn(1)–N(1)#1	107.42(14)	O(3)–Zn(2)–N(6)#2	106.5(3)
N(5)–Zn(1)–N(1)#1	114.40(16)	N(2)#4–Zn(2)–N(6)#2	110.8(4)

Symmetry transformations used to generate equivalent atoms: for **1**: #4 x, -y+3/2, z+1/2; #5 x, -y+1/2, z+1/2; for **2**: #1 x, -y+5/2, z-1/2; #2 x, -y+3/2, z-1/2; for **3**: #1 x, y-1, z; #2 –x+2, -y+1, -z; #3 x+1, y, z; #4 x+1, y+1, z.

Perkin-Elmer Paragon 1000 FT-IR spectrometer. Elemental analyses were performed using a Perkin-Elmer 2400 CHN elemental analyzer. Thermogravimetric analysis (TGA) was performed under nitrogen with a Perkin-Elmer TGA-7 TG analyzer. The powder X-ray diffraction (PXRD) measurements were recorded on a MPD Philips Analytical diffractometer at 40 kV, 30 mA with Cu $K\alpha$ radiation (λ = 1.5406 Å). Brunauer−Emmett−Teller (BET) analyses were investigated with a Micrometrics ASAP 2020 system using nitrogen and hydrogen as the adsorbate at 77 K and carbon dioxide at 195 K, 273 K, and 298 K, respectively.

Synthesis of $\{[Zn_2(azpy)(aip)_2]\cdot 2DMF\}_n$ (1)

A mixture of $Zn(NO_3)_2\cdot 6H_2O$ (30.1 mg, 0.101 mmol), azpy (9.2 mg, 0.05 mmol), and H_2aip (18.1 mg, 0.101 mmol) were dissolved in a solution of dimethylformamide (DMF, 7 mL) and H_2O (1 mL). The mixture was sealed in a glass vial and heated at 50 °C in a water bath for 4 days. Plate-shaped orange crystals of **1** were isolated by filtration, washed with water and ethanol, and dried in air. Yield: 44% (18.9 mg, based on azpy). FT-IR (KBr pellet, cm^{-1}): 3482 (m), 3253 (m), 3140 (m), 1678 (s), 1625 (s,) 1574 (s), 1478 (m), 1441 (m), 1386 (s), 1343 (s), 1248 (m), 1132 (m), 1098 (m), 961 (m), 932 (w), 852 (m), 797 (m), 777 (m), 731 (m), 678 (w), 604 (w), 571 (w), 530 (w). Elemental Analysis Calcd (%) for $C_{16}H_{18}N_4ZnO_6$: 44.92; H, 4.24; N, 13.09; Found: C, 45.05; H, 4.22; N, 13.21. The formula $[Zn_2(azpy)(aip)_2]\cdot 2DMF\cdot 2H_2O$ was assigned based on elemental analysis and thermogravimetric analysis.

Synthesis of $\{[Zn_2(dipytz)(aip)_2]\cdot 1.15DMF\cdot 0.85MeOH\}_n$ (2)

A mixture of $Zn(NO_3)_2\cdot 6H_2O$ (30.1 mg, 0.101 mmol), dipytz (11.7 mg, 0.051 mmol), and H_2aip (18.2 mg, 0.101 mmol) were dissolved in solution of DMF (7 mL), MeOH (1 mL) and EtOH (1 mL). The mixture was sealed in a glass vial and heated at 50 °C in a water bath for 4 days. Plate-shaped red crystals of **2** were isolated by filtration, washed with water and ethanol, and dried in air. Yield: 54% (22.7 mg, based on dipytz). FT-IR (KBr pellets, cm^{-1}): 3438 (m), 3254 (m), 3140 (m), 1667 (s), 1627 (s), 1574 (s), 1478 (m), 1441 (m), 1384 (s), 1342 (s), 1248 (m), 1133 (m), 1099 (m), 961 (m), 927 (w), 795 (m), 777 (m), 731 (m), 685 (w), 604 (w), 571 (w), 536 (w). Elemental Analysis Calcd (%) for $C_{32.3}H_{33.45}N_{9.15}Zn_2O_{12}$: C, 44.45; H, 3.86; N, 14.69%; Found: C, 44.16; H, 4.01; N, 14.82%. The formula $[Zn_2(dipytz)(aip)_2]\cdot 1.15DMF\cdot 0.85MeOH\cdot 2H_2O$ was assigned based on elemental analysis and thermogravimetric analysis.

Synthesis of $\{[Zn_2(tpim)(aip)_2]\cdot 2.5DMF\cdot 2H_2O\}_n$ (3)

A mixture of $Zn(NO_3)_2\cdot 6H_2O$ (29.9 mg, 0.099 mmol), tpim (14.9 mg, 0.049 mmol), and H_2aip (18.1 mg, 0.101 mmol) were

dissolved in a solution of DMF (7 mL), H_2O (1 mL), MeOH (1 mL) and EtOH (1 mL). The mixture was sealed in a glass vial and heated at 50 °C in a water bath for 4 days. Plate-shaped colorless crystals of **3** were isolated by filtration, washed with water and ethanol, and dried in air. Yield: 79% (39.8 mg, based on tpim). FT-IR (KBr pellets, cm^{-1}): 3454 (m), 3262 (m), 3143 (m), 1668 (s), 1621 (s), 1574 (s), 1479 (m), 1441 (m), 1386 (s), 1346 (s), 1133 (m), 1098 (m), 1028 (m), 963 (m), 847 (w), 833 (w), 796 (m), 779 (m), 731 (m), 680 (w), 663 (w), 612 (w), 562 (w), 530(w), 512 (w). Elemental Analysis Calcd (%) for $C_{41.5}H_{45.5}N_{9.5}Zn_2O_{12.5}$: C, 49.49; H, 4.45; N, 13.21%; Found: C, 49.06; H, 4.35; N, 13.13%.

Single-crystal structure analyses

Diffraction measurements for compounds **1**–**3** were carried out using a Brucker SMART APEX CCD diffractometer with grapthite-monochromated Mo *K*α radiation (λ = 0.71073 Å). The crystal structures were solved with direct methods and refined using the SHELXL-97[11] program by full-matrix least-squares on F^2 values. The positions of the C–H hydrogen atoms were generated geometrically and the isotropic thermal parameters were assigned. In **2**, the disordered pyridyl ring of the dipytz ligand were modeled over two occupied sites with refined site occupancy factors of 0.823 (C12A and C13A) and 0.177 (C12B and C13B). The isotropic restraints (ISOR) are applied to DMF and methanol solvents and the atoms of N1, N3, N4, C11, C14, respectively. In **3**, the imidazole rings and pyridyl rings of the tpim ligand are disordered with a 50% site occupancy (Fig. S9†). However, the hydrogen atoms of the lattice water molecule in **3** could not be positioned reliably. Isotropic restraints (ISOR) were applied for water solvents (O10 and O11). Crystal data and structure refinement results for **1**–**3** were listed in Table 1, and the selected bond lengths and angles are given in Table 2.

Results and discussion

Syntheses of 1–3

The reaction of $Zn(NO_3)_2{\cdot}6H_2O$, 5-aminoisophthalic acid (H_2aip) and the pillar ligand, 4,4'-azobipyridine (azpy), di-3,6-(4-pyridyl)-1,2,4,5-tetrazine (dipytz), or 2,4,5-tri(4-pyridyl)-imidazole (tpim), in a 2:2:1 molar ratio at 50 °C for four days resulted in the formation of three Zn(II)-based pillared-bilayer frameworks, $\{[Zn_2(azpy)(aip)_2]{\cdot}2DMF\}_n$ (**1**), $\{[Zn_2(dipytz)(aip)_2]{\cdot}1.15DMF{\cdot}0.85MeOH\}_n$ (**2**), and $\{[Zn_2(tpim)(aip)_2]{\cdot}2.5DMF{\cdot}2H_2O\}_n$ (**3**), as highly crystalline products (Scheme 1).

Description of the crystal structures

Crystal structures of $\{[Zn_2(azpy)(aip)_2]{\cdot}2DMF\}_n$ (1), $\{[Zn_2(dipytz)(aip)_2]{\cdot}1.15DMF{\cdot}0.85MeOH\}_n$ (2), and $\{[Zn_2(Htpim)(aip)_2]{\cdot}2.5DMF{\cdot}2H_2O\}_n$ (3)

Single-crystal X-ray diffraction analyses revealed that compounds **1** and **2** crystallize in the monoclinic space group $P2_1/c$. The asymmetric unit of **1** contains one Zn^{II} ion, one half of the azpy ligand, one aip^{2-} ligand, and one guest DMF molecule. The centre of the −N=N− double bond of the azpy ligand is located about a crystallographic inversion centre. On the other hand, the guest DMF molecule is unequally disordered over the two sites. Each Zn^{II} centre is coordinated to one pyridyl nitrogen atom of the azpy ligand, one amino nitrogen atom of the aip^{2-} ligand, and two monodentate carboxylate oxygen atoms from two different aip^{2-} ligands in a distorted tetrahedral geometry (Fig. 1a). As shown in Fig. 1b, each aip^{2-} ligand is bound to three different Zn^{II} ions by two monodentate carboxylate groups and one amino group [$Zn^{II}\cdots Zn^{II}$ separation of 7.74(16)–8.90(15) Å] (Fig. S1†). Thus, each Zn^{II} ion is surrounded by three bridging aip^{2-} ligands to form a pleated (6,3) honeycomb-like layer with aperture dimensions of 3.4 × 4.9 $Å^2$ (Fig. S2†). In addition, the Zn^{II} ion is further connected to one pillar linker azpy in a tetrahedral fashion, leading to the formation of a pillared-bilayer structure (Fig. 1c). The $Zn^{II}\cdots Zn^{II}$ distance across the azpy bridge is 13.1(30) Å. It is significant that large square-shaped channels were observed within the framework along the *b* axis with effective dimensions of 4.1 × 10.1 $Å^2$ (Fig. 1d). Smaller

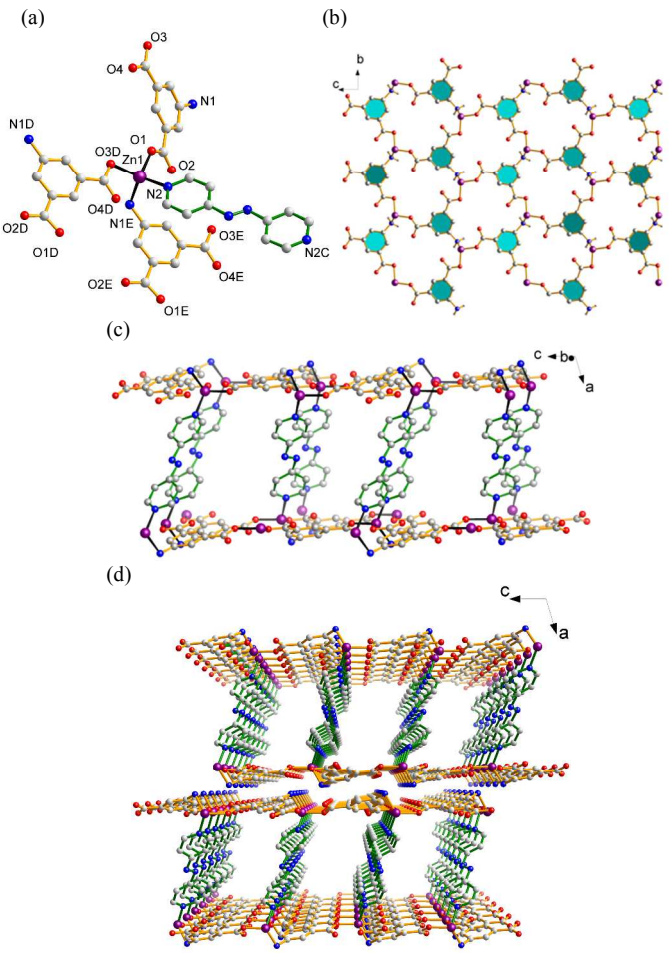

Fig. 1 (a) Coordination environments of the Zn^{II} ion in **1**. (b) A perspective view of the pleated layer in **1**. (c) 2D pillared-bilayer network of **1** along the *b* axis. (d) The pillared-bilayer network of **1** showing large 1D channels observed along the *b* axis. Symmetry transformations used to generate equivalent atoms: (C) -x+1,-y,-z+1; (D) x, -y+3/2, z+1/2; (E) x, -y+1/2, z+1/2.

channels were also observed along the *c* axis with dimensions of 3.1 × 4.3 Å^2 (Fig. S3a†). Analysis using the PLATON[12] software indicated that the extra-framework volume per unit cell is approximately 35.7%.

Compounds **1** and **2** differ from one another only from the pillar linkers and lattice guest molecule. The asymmetric unit of **2** contains one Zn^{II} ion, one half of a dipytz ligand, one aip^{2-} ligand, one half of a guest DMF, and half of a guest MeOH molecule. The centre of the dipytz ligand is located about a crystallographic inversion centre. The guest DMF molecule is in general position with the site occupancy factor refined to be 0.575. In addition, the guest methanol molecule is in general position with the site occupancy factor refined to be 0.425. The Zn^{II} centre adopts the same distorted tetrahedral coordination environments in **1** (Fig. 2a). The layers in compound **2** have the same connection mode as that in **1**, while the bond distances changed because the azpy ligand is replaced by the dipytz ligand. As a consequence, the dipytz ligand acts as a pillar to support the infinite 2D layers, thus leading to an extended 2D pillared-bilayer structure with a Zn···Zn separation distance of 15.1(18) Å (Fig. 2b). The large square-shaped channels were observed within the framework along the *b* axis with effective dimensions of 4.1 × 11.1 Å^2 and smaller channels are also observed along the *c* axis with dimensions of 4.3 × 4.4 Å^2 (Fig. 2c and S4a†). Analysis using the PLATON software indicated that the extra-framework volume per unit cell is approximately 41.7%.

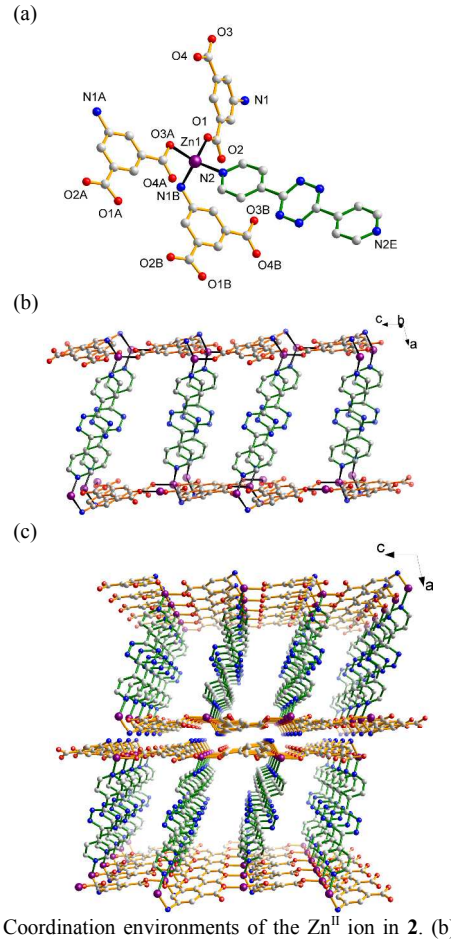

Fig. 2 (a) Coordination environments of the Zn^{II} ion in **2**. (b) 2D pillared-bilayer network of **2** along the *b* axis. (c) Pillared-bilayer network of **2** showing large 1D channels along the *b* axis. Symmetry transformations used to generate equivalent atoms: (A) x, -y+5/2, z-1/2; (B) x, -y+3/2, z-1/2; (E)-x+1, -y+1, -z.

Compound **3** crystallizes in the monoclinic space group $P2_1/n$ and also adopts a pillared-bilayer structure. The asymmetric unit of **3** contains two Zn^{II} ions, one tpim ligand, two aip^{2-} ligands, two and one half guest DMF molecules, and two guest water molecules. Both Zn(1) and Zn(2) centres adopt distorted tetrahedral coordination environments (Fig. 3a). Each Zn^{II} ion is bridged by an aip^{2-} ligand to produce a 2D layer with the same connection mode as in **1** and **2**. Interestingly, the tpim ligand possesses three pyridine groups but only two of them ligand serve as pillars to interlink a pair of layers to create 1D

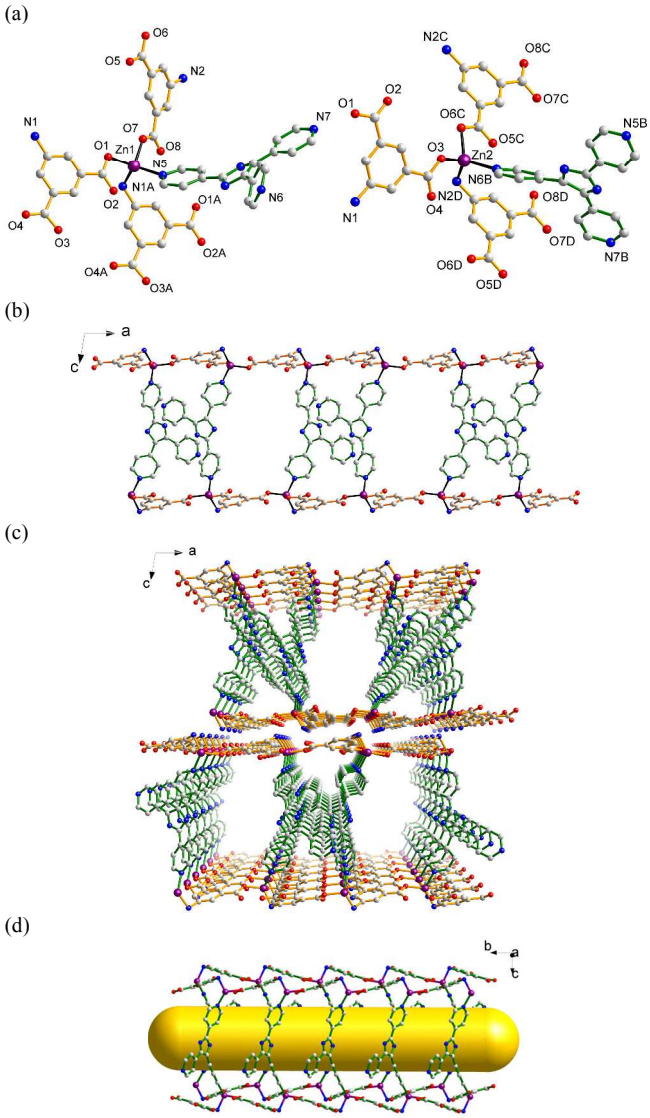

Fig. 3 (a) Coordination environments of the Zn^{II} ion in **3**. (b) 2D pillared-bilayer network of **3** along the *b* axis. (c) The pillared-bilayer network of **3** showing large 1D channels along the *b* axis. (d) A 1D channel of 5.8 × 9.1 Å^2 (highlighted in yellow) along the *b* axis. Symmetry transformations used to generate equivalent atoms: (A) x, y-1, z; (B) -x+2, -y+1, -z; (C) x+1, y, z; (D) x+1, y+1, z.

channels inside the bilayers (Fig. 3b). The 1D rhombic-shaped channels can be observed along the *b* axis with dimensions of 5.1 × 9.8 Å^2 (Fig. 3c). The $Zn^{II}\cdots Zn^{II}$ separation distance across the tpim bridge is 13.6(9) Å. The channels were occupied by guest DMF and water molecules. Analysis using the PLATON software indicated that the extra-framework volume per unit cell is approximately 33.9%.

For all of the frameworks, the neighboring 2D layers are same packed by fitting the grooves together and are extended to a 3D supramolecular framework by two types of hydrogen bonding interactions between the amino group and carboxylate oxygen atoms. Meanwhile, there are strong π–π stacking interactions between the benzene rings of the interlayers with a face-to-face distance of 3.7(1)–3.8(1) Å (Fig. S6†). To identify the topology of the pillared-bilayer network, the aip^{2-} ligand can be assigned as a three-connected node assuming that it bridges three metal ions, and each metal ion can be assumed to be a four-connected node because it coordinates to three aip^{2-} ligands and one pillar linker. The overall array of the frameworks result in a (3,4)-connected topological network with a point symbol of $\{6^3\}\{6^6\}$ (Fig. 4).[13]

Although the constructions of the pillared-bilayer MOFs in **1**–**3** are similar, based on the 2D lamina, it should be noted that

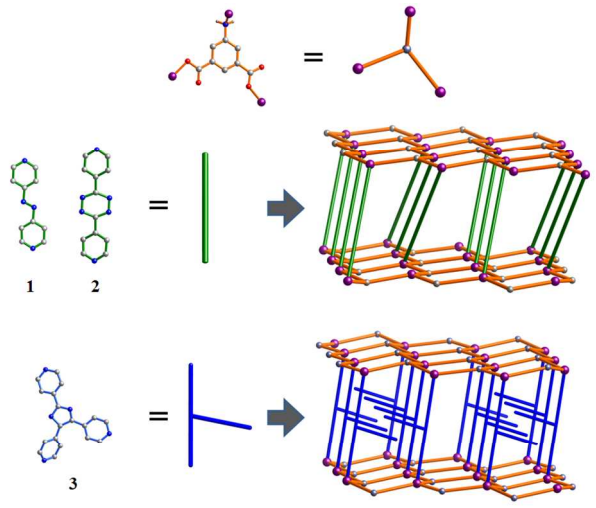

Fig. 4 A simplified view of the pillared-bilayer networks of **1**–**3**.

there are structural differences between them. The *β* angles of the monoclinic cell of **1**–**3** are 106.4(3)°, 102.3(2)°, and 99.7(13)°, respectively, with the reflection corresponding to an adjacent 2D layer by the bridged ligands. In the cases of **1** and **2**, we attempted to increase the length of the pillar ligands to increase the porosity of the frameworks. In compound **3**, the uncoordinated pyridyl group of the tpim ligand caused a reduction in the inner cavity space, but large one-dimensional channels were formed. Furthermore, the pillaring ligands azpy, dipytz, and ptim successfully modulate the size and shape of the channel spaces of the resulting arrays of networks. On the basis of the structures of **1** and **2**, two linear-shaped pillaring ligand azpy and dipytz provided −N=N− and tetrazine functional group decorated the channel surface, respectively. It is noteworthy that in the case of compound **3**, some significant features are: (1) only two pyridyl groups of the tpim ligand are coordinated to the metal centres that support the $[Zn(aip)]_n$ layers, therefore, the third pyridyl group resembles a pendent arm and the imidazole moiety serves as a functional decoration of the channel wall; (2) the tpim ligand is able to participate in strong π–π interactions between the regularly arranged tpim pillars, thus enhancing the rigidity of the resulting pillared-bilayer host of **3** (Fig. S8†). Pillared-bilayer MOFs are rare in the literature and several are listed in Table 3. More importantly, the results of this study revealed that the 2D pillared-bilayer structures can be systematically synthesized and allow open frameworks with tunable pore sizes and shapes to produced when appropriate functionalized pillar ligands are employed.

Thermogravimetric analyses

Thermogravimetric analyses (TGA) of **1** revealed a weight loss of 4.2% (calculated 3.7%) in the range of 25–40 °C, which correspond to a loss of two H_2O molecules. A second weight loss of 17.5% (calculated 17.6%) was then observed in the range of 40–158 °C, corresponding to the release of two DMF molecules and the entire structure begins to decompose, eventually collapsing at 300 °C. The TGA curve for **2** revealed a weight loss of 8.6% (calculated 7.3%) during the first step from 25 to 88 °C corresponding to the loss of two guest water molecules and methanol molecule, and a second weight loss of 8.2% (calculated 9.6%) was observed in the range of 88–158 °C, corresponding to the release of DMF molecule. The framework

Table 3 The modulation of the pillar-functionalized bilayer array networks

Compound	**1**	**2**	**3**	Ref. 6a	Ref. 6a	Ref. 5c
Pillar ligands	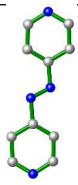		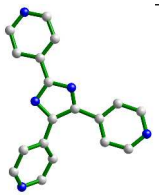	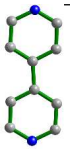	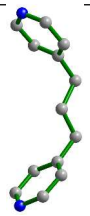	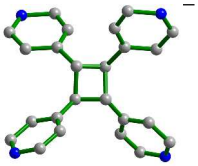
Channel sizes (Å^2)	4.1 × 10.1 3.1 × 4.3	4.1 × 11.1 4.3 × 4.4	5.1 × 9.8	3.5 × 6.7 2.1 × 4.1	3.9 × 7.8	×
Solvent accessible area	35.7%	41.7%	33.9%	20.7%	25.5%	7.8%

began to decompose with a continuous weight loss at temperatures over 290 °C, which can be attributed to the loss of the coordinating ligands. The TGA profile for **3** revealed a weight loss of 19.8% (calculated 21.6%) in the range of 25–190 °C, which can be attributed to the loss of the guest water and DMF molecules (Fig. S9†). The framework is stable up to 420 ºC.

Powder X-ray diffraction analyses

Powder X-ray diffraction (PXRD) were used to confirm the phase purity of **1–3** as well as their stability upon solvent-exchanged processes. The results showed that all peaks were in good agreement with the corresponding simulated patterns (Fig. S10–S12†). Furthermore, the patterns of the methanol-exchanged samples retained an acceptable degree of crystallinity (Fig. S13–S15†). The PXRD patterns of the methanol-exchanged **1** and **2** were slightly different from those of the as-synthesized samples, suggesting the possibility that **1** and **2** are structurally flexible. For the compound **3**, the peaks for the methanol-exchanged sample were slightly shifted from the simulated peak positions but the crystallinity was maintained, which indicated that compound is more rigid and retains its stability after guest exchange. A schematic representation of the structural transformation upon guest exchange is shown in Scheme 2.[14]

Scheme 2 Schematic representation of the structural transformation upon solvent-exchanged process in the 2D pillared-bilayer networks with 1D channels.

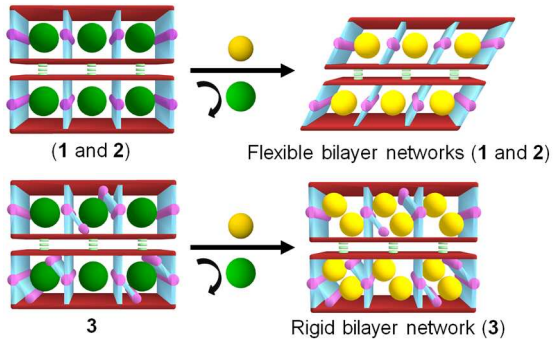

Gas adsorption studies

In order to explore the gas sorption properties of the pillared-bilayer frameworks, freshly prepared samples were immersed in methanol for 2 days at room temperature to allow the solvents to be exchanged. The guests-exchanged compounds were confirmed by the disappearance of a strong DMF C=O stretching peak at 1668 cm^{-1} in the IR spectrum (Fig. S17†). All of these compounds were desolvated at 120 °C overnight under a vacuum. The results were verified by TGA analyses, which showed that the guest DMF molecules in **1–3** had been completely exchanged and removed. Gas sorption experiments of compounds **1–3** were carried out under atmospheres of nitrogen, hydrogen, and carbon dioxide, respectively, to investigate their pore properties and gas storage capabilities. The activated samples, after removing the methanol remained stable and no appreciable amount of mass was lost until it undergoes decomposition (Fig. S16†). The results indicated that activated compounds **1–3** adsorbed only a minor amount of N_2 at 77 K and 1 atm (Fig. S18†). N_2 molecules did not diffuse into the channels in compounds **1–3**, this may be due to possible framework contraction and the absence of appropriate intermolecular interactions at low temperature.

The adsorption isotherms for CO_2 in **1–3** at 195 K showed type I adsorption behavior, which are characteristic of microporous materials (Fig. 5). To our surprise, adsorption measurements showed that the total amount CO_2 taken up by **1–3** was 53.1, 89.9, and 121.7 $cm^3\ g^{-1}$, respectively, with apparent Brunauer−Emmett−Teller (BET) surface areas of 132, 248, and 317 $m^2\ g^{-1}$ (Langmuir surface areas of 239, 400, and 539 $m^2\ g^{-1}$). Significantly, compound **3** showed a larger CO_2 adsorption capacity than compounds **1** and **2**. In addition, the CO_2 adsorption value for **3** was higher than that of many previously reported 2D porous MOFs.[15] In the case of **1** and **2**, the smaller pore volume as well as the lesser void space, as calculated by PLATON, was also reflected in the lower uptake of CO_2. This can be attributed to the decreased length of the linear-shaped pillar linkers as well as the flexible nature of the pillared-bilayer structure. In compound **3**, the π–π stacking interactions of the dangling arm of the ptim linker significantly strengthened the rigidity of the pillared-bilayer network. Furthermore, the imidazole moiety as well as the uncoordinated pyridyl group of the pillar ligand in the channels of compound **3** also facilitated interactions with respect to CO_2 molecules.[16]

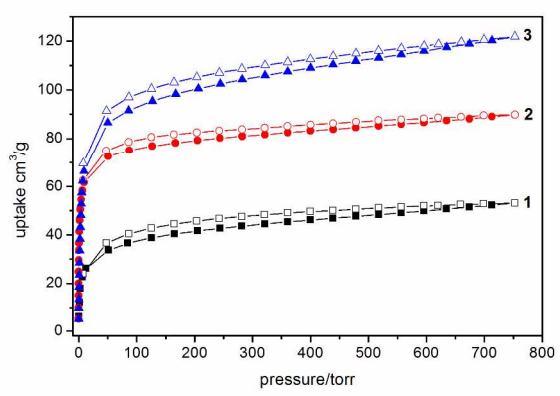

Fig. 5 The CO_2 adsorption isotherms of **1–3** at 195 K.

The adsorption isotherms for H_2 were probed in **1–3** at 77 K. The maximum amounts of H_2 taken up were 14.3, 6.5, and 55.7 $m^3\ g^{-1}$ for **1–3**, respectively. Interestingly, compound **3** showed the greatest H_2 uptake as compared to compounds **1** and **2**, and displayed a reversible type I adsorption in this series (Fig. 6). The sorption isotherm of **3** also displays a mall hysteresis, which revealed strong interactions between H_2 and the host framework. On the contrary, the networks of **1** and **2** were less effective for hydrogen adsorption, possibly due to framework contraction and the absence of appropriate intermolecular interactions at low temperature.

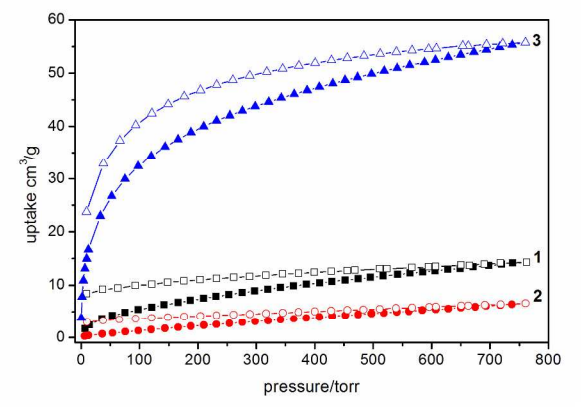

Fig. 6 The H_2 adsorption isotherms of **1–3** at 77 K.

To better understand the adsorption properties of compounds **1–3**, the heats of adsorption (Q_{st}) of the CO_2 adsorption isotherms were calculated at 273 K and 298 K by using both the virial fitting method and Clausius−Claperyron equation.[17] As shown in Fig 7, at zero loading, the Q_{st} values ($-\Delta H$) for compounds **1–3** were determined to be 36.8, 24.1 and 29.5 kJ mol^{-1}, respectively, showing a steady retention at higher coverages. The Q_{st} value of **1** was the highest compared to reported pervious microporous 2D MOFs, in which the pore surfaces are decorated by −N=N− functional groups (20 kJ mol^{-1}).[18] Interestingly, compound **1** possessed the greatest Q_{st} value compared to compound **2**, suggesting that the narrow pore size and pore surface (decorated with a −N=N− group) facilitates the optimization of the CO_2−framework and adsorbate−adsorbent interactions within the 1D channels.[19] On the other hand, compound **3** showed higher CO_2 and H_2 uptake capacities than those of compounds **1** and **2**, indicating that the rigidity and stability of the pillar-bilayer networks is an important factor for effective gas adsorption. In short, by modulating the pillar-functionalized pores in the series of compounds **1–3**, it was possible to successfully tune the porosity, the functionality, rigidity (flexibility) and selectivity of such materials for gas adsorption.

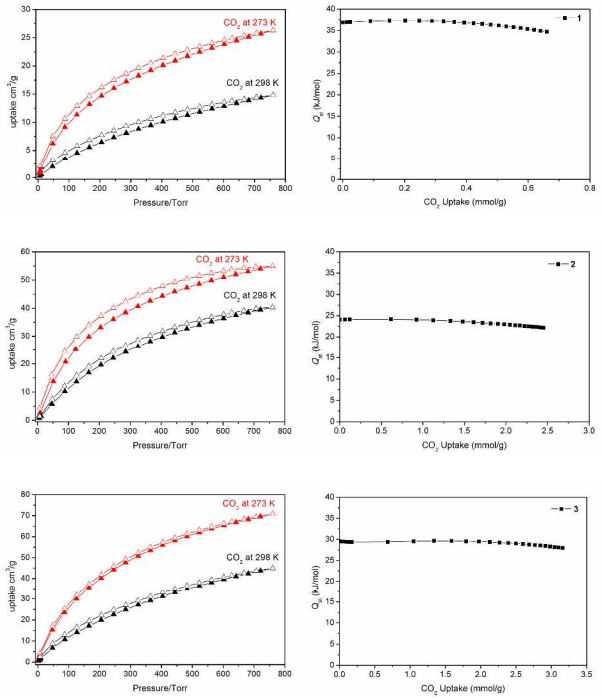

Fig. 7 CO_2 adsorption isotherms at 273 K and 298 K (left) and the isosteric heats (Q_{st}) of CO_2 adsorptions (right) for **1–3**.

Conclusions

We systemically synthesized three pillared-bilayer Zn(II)–organic frameworks, in which 2D layers were connected by functionalized pillared ligands. The resulting MOFs show tunable structures, as their pore size and rigidity (flexibility) could be controlled by adjusting the length, shape and functionality of the pillared ligands. Their structural characteristics allow these pillared-bilayer MOFs to serve as excellent models for studies of gas adsorption properties.

Acknowledgements

We are grateful to Academia Sinica, National Central University and the Ministry of Science and Technology of Taiwan for financial support.

Notes and references

[a] *Institute of Chemistry, Academia Sinica, Taipei 115, Taiwan. Tel: 886-2-27898518; E-mail: kllu@gate.sinica.edu.tw*
[b] *Institute of Materials Science and Engineering, National Central University, Taoyuan 320, Taiwan*
[c] *Department of Chemistry, Fu Jen Catholic University, Taipei 242, Taiwan*
[d] *Department of Chemistry, National Taiwan University, Taipei 107, Taiwan*

†Electronic Supplementary Information (ESI) available: additional figures for the crystal structures, TGA spectra, FTIR spectra, PXRD patterns and Figs. S1−S21. CCDC: 1063484-1063486
See DOI: 10.1039

1 (*a*) S. Kitagawa, R. Kitaura and S. i. Noro, *Angew. Chem., Int. Ed.*, 2004, **43**, 2334; (*b*) T. T. Luo, H. L. Tsai, S. L. Yang, Y. H. Liu, R. D. Yadav, C. C. Su, C. H. Ueng, L. G. Lin and K. L. Lu, *Angew. Chem., Int. Ed.*, 2005, **44**, 6063; (*c*) Y. Z. Zheng, M. L. Tong, W. Xue, W. X. Zhang, X. M. Chen, F. Grandjean and G. J. Long, *Angew. Chem., Int. Ed.*, 2007, **46,** 6076; (*d*) M. O'Keeffe and O. M. Yaghi, *Chem. Rev.*, 2012, **112**, 675; (*e*) X. S. Wang, M. Chrzanowski, W. Y. Gao, L. Wojtas, Y. S. Chen, M. J. Zaworotko and S. Ma, *Chem. Sci.*, 2012, **3**, 2823.

2 (*a*) R. E. Morris and P. S. Wheatley, *Angew. Chem., Int. Ed.*, 2008, **47**, 4966; (*b*) L. J. Murray, M. Dincă and J. R. Long, *Chem. Soc. Rev.*, 2009, **38**, 1294; (*c*) A. Phan, C. J. Doonan, F. J. Uribe-Romo, C. B. Knobler, M. O'Keeffe and O. M. Yaghi, *Acc. Chem. Res.*, 2010, **43**, 58; (*d*) J. R. Li, J. Sculley and H. C. Zhou, *Chem. Rev.*, 2012, **112**,

869; (*e*) Y. Yan, S. Yang, A. J. Blake, and M. Schröder, *Acc. Chem. Res.* 2014, **47**, 296.

3 (*a*) M. Zhao, S. Ou and C. D. Wu, *Acc. Chem. Res.*, 2014, **47**, 1199; (*b*) M. Yoon, R. Srirambalaji and K. Kim, *Chem. Rev.*, 2012, **112**, 1196; (*c*) S. Yang, L. F. Liu, J. L. Sun, K. M. Thomas, A. J. Davies, M. W. George, A. J. Blake, A. H. Hill, A. N. Fitch, C. C. Tang, and M. Schröder, *J. Am. Chem. Soc.*, 2013, **135**, 4954.

4 (*a*) M. D. Allendorf, C. A. Bauer, R. K. Bhakta and R. J. T. Houk, *Chem. Soc. Rev.*, 2009, **38**, 1330; (*b*) L. E. Kreno, K. Leong, O. K. Farha, M. Allendorf, R. P. V. Duyne, and J. T. Hupp, *Chem. Rev.*, 2012, **112**, 1105.

5 (*a*) H. J. Choi and M. P. Suh, *J. Am. Chem. Soc.*, 2004, **126**, 15844; (*b*) K. L. Gurunatha, S. Mohapatra, P. A. Suchetan and T. K. Maji, *Cryst. Growth Des.*, 2009, **9**, 3844; (*c*) M. Dai, W. Y. Yan, Z. G. Ren, H. F. Wang, W. J. Gong, F. L. Li, X. Zhao, H. X. Li and J. P. Lang, *CrystEngComm*, 2012, **14**, 6230; (*d*) Z. Yin, Y. L. Zhou, M. H. Zeng and M. Kurmoo, *Dalton Trans.*, 2015, **44**, 5258.

6 (*a*) K. O. Kongshaug and H. Fjellvåg, *Inorg. Chem.*, 2006, **45**, 2424; (*b*) J. T. Shi, C. S. Zhou, Y. L. Liu, Z. G. Fang, R. L. Zhao, L. L. Xu and K. F. Yue, *Z. Anorg. Allg. Chem.*, 2013, **639**, 187; (*c*) R. Haldara and T. K. Maji, *CrystEngComm*, 2013, **15**, 9276; (*d*) X. L. Wang, F. F. Sui, H. Y. Lin, J. W. Zhang and G. C. Liu, *Cryst. Growth Des.*, 2014, **14**, 3438.

7 (*a*) T. K. Maji, K. Uemura, H. C. Chang, R. Matsuda and S. Kitagawa, *Angew. Chem., Int. Ed.*, 2004, **43**, 3269; (*b*) H. Ren, T. Y. Song, J. N. Xu, S. B. Jing, Y. Yu, P. Zhang and L. R. Zhang, *Cryst. Growth Des.*, 2009, **9**, 105; (*c*) Z. Chang, D. S. Zhang, Q. Chen, R. F. Li, T. L. Hu and X. H. Bu, *Inorg. Chem.*, 2011, **50**, 7555; (*d*) S. Henke, A. Schneemann, A. Wütscher and R. A. Fischer, *J. Am. Chem. Soc.*, 2012, **134**, 9464; (*e*) J. T. Culp, C. Madden, K. Kauffman, F. Shi and C. Matranga, *Inorg. Chem.*, 2013, **52**, 4205. (*f*) C. H. Lee, J. Y. Wu, G. H. Lee, S. M. Peng, J. C. Jiang and K. L. Lu, *Cryst. Growth Des.*, 2014, **14**, 5608; (*g*) X. L. Zhao, F. L. Liu, L. L. Zhang, D. Sun, R. M. Wang, Z. F. Ju, D. Q. Yuan and D. F. Sun, *Chem. Eur. J.*, 2014, **20**, 649.

8 J. P. Launay, M. Tourrel-Pagis, J. F. Lipskier, V. Marvaud and C. Joachim, *Inorg. Chem.*, 1991, **30**, 1033.

9 P. H. Dinolfo, M. E. Williams, C. L. Stern and J. T. Hupp, *J. Am. Chem. Soc.*, 2004, **126**, 12989.

10 M. V. Proskurnina, N. A. Lozinskaya, S. E. Tkachenko and N. S. Zefirov, *Russ. J. Org. Chem.*, 2002, **38**, 1149.

11 G. M. Sheldrick, A Short History of SHELX, *Acta Cryst.*, 2008, **A64**, 112.

12 A. L. Spek, *J. Appl. Crystallogr.*, 2003, **36**, 7.

13 M. Dai, W. Y. Yan, Z. G. Ren, H. F. Wang, W. J. Gong, F. L. Li, X. Zhao, H. X. Li and J. P. Lang, *CrystEngComm*, 2012, **14**, 6230.

14 (*a*) S. Kitagawa and K. Uemura, *Chem. Soc. Rev.*, 2005, **34**, 109; (*b*) Y. Kubota, M. Takata, R. Matsuda, R. Kitaura, S. Kitagawa and T. C. Kobayashi, *Angew. Chem. Int. Ed.*, 2006, **45**, 4932; (*c*) A. Kondo, H. Kajiro, H. Noguchi, L. Carlucci, D. M. Proserpio, G. Ciani, K. Kato, M. Takata, H. Seki, M. Sakamoto, Y. Hattori, F. Okino, K. Maeda, T. Ohba, K. Kaneko and H. Kanoh, *J. Am. Chem. Soc.*, 2011, **133**, 10512; (*d*) Z. H. Xuan, D. S. Zhang, Z. Chang, T. L. Hu and X. H. Bu, *Inorg. Chem.*, 2014, **53**, 8985.

15 (*a*) T. K. Maji, G. Mostafa, R. Matsuda and S. Kitagawa, *J. Am. Chem. Soc.*, 2005, **127**, 17152; (*b*) P. Kanoo, G. Mostafa, R. Matsuda, S. Kitagawa and T. K. Maji, *Chem. Commun.*, 2011, **47**, 8106; (*c*) S. Parshamoni, S. Sanda, H. S. Jena and S. Konar, *Dalton Trans.*, 2014, **43**, 7190.

16 (*a*) J. B. Lin, W. Xue, J. P. Zhang and X. M. Chen, *Chem. Commun.*, 2011, **47**, 926; (*b*) W. Y. Gao, W. Yan, R. Cai, K. Williams, A. Salas, L. Wojtas, X. Shi and S. Ma, *Chem. Commun.*, 2012, **48**, 8898; (*c*) P. Z. Li, X. J. Wang, R. H. D. Tan, Q. Zhang, R. Q. Zou and Y. L. Zhao, *RSC Adv.*, 2013, **3**, 15566.

17 J. L. C. Rowsell and O. M. Yaghi, *J. Am. Chem. Soc.*, 2006, **128**, 1304.

18 (*a*) P. Kanoo, A. C. Ghosh, S. T. Cyriac and T. K. Maji, *Chem. Eur. J.*, 2012, **18**, 237; (*b*) N. Sikdar, A. Hazra and T. K. Maji, *Inorg. Chem.*, 2014, **53**, 5993.

19 (*a*) C. M. Nagaraja, R. Haldar, T. K. Maji and C. N. R. Rao, *Cryst. Growth Des.*, 2012, **12**, 975; (*b*) B. Bhattacharya, R. Dey, P. Pachfule, R. Banerjee and D. Ghoshal, *Cryst. Growth Des.*, 2013, **13**, 731; (*c*) B. Bhattacharya, D. Saha, D. K. Maity, R. Dey and D. Ghoshal, *CrystEngComm*, 2014, **16**, 4783.

Journal Name

RSCPublishing

ARTICLE

Graphical Abstract

Pillared-bilayer zinc(II)–organic laminae: pore modification and selective gas adsorption

Li-Wei Lee, Tzuoo-Tsair Luo, Sheng-Han Lo, Gene-Hsiang Lee, Shie-Ming Peng, Yen-Hsiang Liu,* Sheng-Long Lee* and Kuang-Lieh Lu*

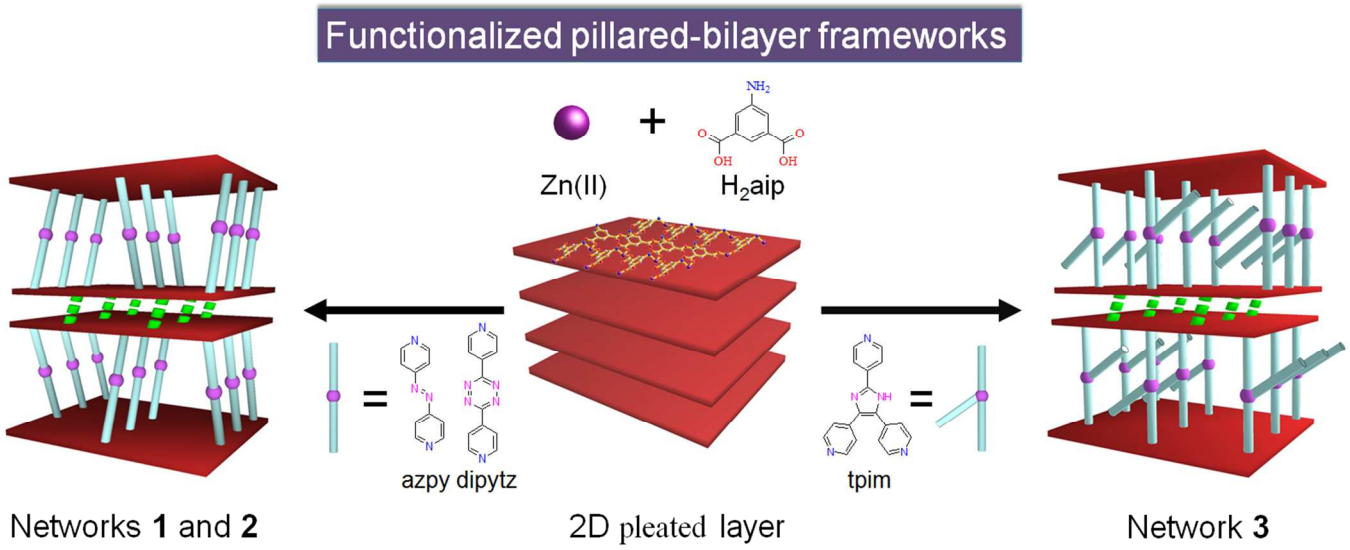

Three Zn(II)-based pillared-bilayer MOFs were systematically synthesized. Their unusual structural characteristics allow these pillared-bilayer MOFs to serve as excellent models for studies of gas adsorption properties.